Research Article Vol. 33, No. 25 / 15 Dec 2025 / Optics Express 51782
Optics EXPRESS

Diode-pumped continuous-wave Yb:YVO_4 laser with a broad tuning range of 986 to 1119 nm

MUHARREM KILINC,[1,2] UMIT DEMIRBAS,[1,3,4] MARTIN KELLERT,[1] JELTO THESINGA,[1] ALEXEY YAKOVLEV,[1] MIKHAIL PERGAMENT,[1] AND FRANZ X. KÄRTNER[1,5,6,*]

[1]*Center for Free-Electron Laser Science CFEL, Deutsches Elektronen-Synchrotron DESY, Notkestr. 85, 22607 Hamburg, Germany*
[2]*Institute for Particle Physics and Astrophysics, ETH Zurich, 8093 Zurich, Switzerland*
[3]*Department of Electrical and Electronics Engineering, Antalya Bilim University, 07190 Dosemealti, Antalya, Turkey*
[4]*Paul Scherrer Institute, Forschungsstrasse 111, 5232 Villigen, Switzerland*
[5]*Physics Department, University of Hamburg, Luruper Chaussee 149, 22761 Hamburg, Germany*
[6]*The Hamburg Centre for Ultrafast Imaging, Luruper Chaussee 149, 22761 Hamburg, Germany*
[*]*franz.kaertner@desy.de*

Abstract: We present a diode-pumped continuous-wave (CW) Yb:YVO_4 laser exhibiting wavelength tunability from 986 nm to 1119 nm, corresponding to a broad tuning range of 133 nm, one of the widest reported for any Yb-doped laser host. This performance was achieved by employing a low-loss, off-surface optic-axis birefringent filter, high-quality laser crystals, and optimized low-loss cavity optics, enabling smooth and stable wavelength tuning along both principal polarization axes (E//a: 986-1084 nm and E//c: 995-1119 nm). The system delivers CW output powers up to 3.75 W, with slope and optical-to-optical efficiencies reaching 70% and 48%, respectively. These results highlight Yb:YVO_4 as an attractive gain medium for applications requiring broad tunability, compactness, and efficiency, such as ultrafast pulse generation, broadband spectroscopy, and high-energy amplifier seeding.

1. Introduction

Tunable lasers find extensive applications in various fields, including spectroscopy, biomedical imaging, material processing, remote sensing [1–6]. Ytterbium-doped host materials provide relatively broad tuning near 1.05 μm (Fig. 1) and attract considerable attention due to their power and energy scalability. Among the alternatives, Yb:YVO_4 stands out as one of the few that could be tuned to shorter wavelengths, even below 1 μm, which is a promising wavelength region for seeding of cryogenic Yb:YLF amplifiers with strong gain peaks around 995, 1016 and 1018 nm [7]. Because of its blue-shifted gain spectrum [8–10], Yb:YVO_4 also emerges as a promising platform for generating sub-100-fs pulses at these shorter wavelengths, well aligned with our effort to develop Joule-class, kHz-rate cryogenic Yb:YLF amplifiers [11], (see Fig. 1 in [12]).

To our knowledge, lasing in Yb:YVO_4 was demonstrated for the first time by Kisel et al. in 2004, where a CW power up to 0.61 W was achieved at 1020 nm with a slope efficiency close to 50% under diode pumping at 984 nm [8]. Kisel et al. also investigated the laser-related spectroscopic properties of 1.62% Yb-doped YVO_4 and determined its room temperature fluorescence lifetime (τ) and peak fluorescence emission cross section (σ_{em}) at 1008 nm as, 247 μs and 1.25×10^{-20} cm^2, respectively [8]. Compared to the well-known Yb:YAG, the fluorescence lifetime of Yb:YVO_4 is approximately 3.8-fold shorter, and its peak emission cross-section is around 1.7-fold smaller, resulting overall in about a 6-fold lower gain product ($\tau\sigma_{em} \sim 0.3 \times 10^{-23}$ cm^2s). The

#580835 https://doi.org/10.1364/OE.580835
Journal © 2025 Received 2 Oct 2025; revised 19 Nov 2025; accepted 20 Nov 2025; published 1 Dec 2025

Optics EXPRESS

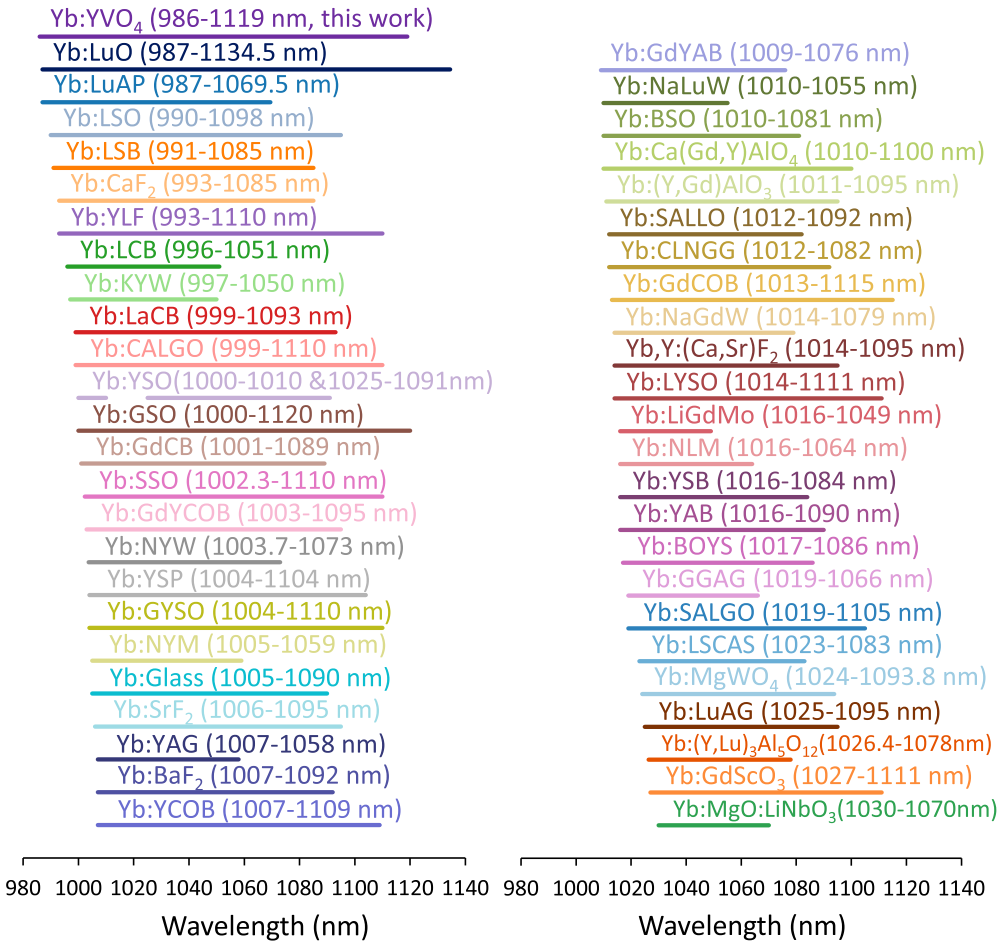

Fig. 1. Summary of continuous wave tuning ranges demonstrated with Yb-based solid-state laser gain media: Yb:LuO [21], Yb:LuAP [22], Yb:LSO [23,24], Yb:LSB [25], Yb:CaF_2 [26], Yb:YLF [27], Yb:LCB [28], Yb:KYW [29], Yb:LaCB [30], Yb:CALGO [31,32], Yb:YSO [23,33], Yb:GSO [34], Yb:GdCB [35], Yb:SSO [36,37], Yb:GdYCOB [38], Yb:NYW [39], Yb:YSP [40,41], Yb:GYSO [42], Yb:NYM [43], Yb:Glass [44–46], Yb:SrF_2 [47], Yb:YAG [48,49], Yb:BaF_2 [50], Yb:YCOB [51], Yb:GdYAB [52], Yb:NaLuW [53], Yb:BSO [54], Yb:$Ca(Gd,Y)AlO_4$ [55], Yb:$(Y,Gd)AlO_3$ [56], Yb:SALLO [57], Yb:CLNGG [58], Yb:GdCOB [59], Yb:NaGdW [60], Yb,Y:$(Ca,Sr)F_2$ [61], Yb:LYSO [62,63], Yb:LiGdMo [64], Yb:NLM [65], Yb:YSB [66], Yb:YAB [67], Yb:BOYS [68], Yb:GGAG [69], Yb:SALGO [70], Yb:LSCAS [71], Yb:$MgWO_4$ [72], Yb:LuAG [73,74], Yb:$(Y,Lu)_3Al_5O_{12}$ [75], Yb:$GdScO_3$ [76], Yb:MgO:$LiNbO_3$ [77]. For each host, the plotted span is the union of the tuning ranges over all accessible polarizations and/or crystal orientations.

thermal conductivity of YVO_4 crystal (5.23 W/(m·K) [8]) is also around one-half of the YAG host. Despite these limitations, Yb:YVO_4 remains attractive due to its broader and smoother gain profile, which enables wider wavelength tuning and shorter pulse generation compared to Yb:YAG.

Table 1 summarizes previous CW lasing results obtained with Yb:YVO_4 lasers. The performance has steadily improved with advancements in pumping techniques, crystal doping

Optics EXPRESS

concentrations, and optimized resonator configurations. CW powers as high as 8.6 W [13] and 10 W [14] have been reported using slab and thin-disk geometries, respectively. Additionally, slope efficiencies exceeding 70% are commonly achievable, with the highest reported being 76% using a simple plano-concave resonator under diode pumping at 985 nm [15]. However, the majority of these previous studies primarily focused on achieving high power levels and improved efficiencies, often within relatively limited tuning ranges typically not exceeding 50 nm. For example, extensive tuning investigations were rarely performed, with most efforts limited to relatively narrow spectral windows (e.g., 1020-1047 nm [16] or 997-1074 nm [13]). Systematic studies that fully explore the broad tuning capabilities offered by the Yb:YVO_4 gain medium across its entire emission bandwidth have thus far been lacking.

Table 1. Summary of CW lasing results obtained with Yb:YVO_4 gain media.

Crystal Yb-doping, length, and lasing configuration	Slope efficiency (%)	Opt-to-opt efficiency (%)	Output power (W)	Tuning range (nm)	Reference
1.62%, 2.44 mm, //c,	49	24	0.61	1020	[8]
1.6%, 1.24 mm, //c	41.1	36	0.433	1037	[9]
3%, 1.76 mm, //c	59	47	0.98	1023	[17]
1.5%, 0.25 mm, //c	43	26	10	1013-1023	[14]
3%, 2 mm, //c	50	47	1.17	1010-1060	[18]
0.8%, 3 mm, //c	61	46.4	7.05	1020-1047	[16]
0.8%, 3 mm, //a	30	26.8	3.75	1021-1036	
0.8%, 2 mm, //c	76	40	2.46	1022-1056	[15]
0.5%, 3 mm, //c	68	40.6	2.65	1017-1042	[19]
2%, 4 mm, //c	57.9	50	8.6	997-1074	[13]
2.6%, 5 mm, //c	70	48	3.75	995-1119	This work
2.6%, 5 mm, //a	50	32	2.41	986-1084	

In this work, we have systematically investigated the CW lasing performance and broad wavelength tuning capabilities of diode-pumped Yb:YVO_4 lasers. Leveraging a cost-effective, single-emitter multimode diode providing up to 10 W output power at 952 nm, we explored lasing along both principal polarization axes (E//a and E//c) across three distinct crystal configurations, enabling a comprehensive evaluation of their performance. By combining low-loss laser crystals, optimized cavity optics, and an innovative off-surface optic-axis birefringent filter [20], we achieved robust CW operation with output powers up to 3.75 W, a slope efficiency of 70%, and optical-to-optical efficiency of 48% using a 2.6%-doped, right-angle-cut Yb:YVO_4 crystal in the E//c configuration. Significantly extending beyond previous studies, we demonstrated smooth, stable, and exceptionally broad CW wavelength tuning over a 133 nm range (986-1119 nm).

Figure 1 summarizes the CW tuning ranges of various Yb-doped solid-state laser hosts. For each gain medium, the tuning ranges of all crystal orientations are combined, since both polarizations can be accessed within a single cavity using a simple half-wave plate and polarizer configuration, without altering the cavity optics. For Yb:YVO_4, the two polarization-dependent tuning ranges (986-1084 nm for E//a and 995-1119 nm for E//c) are both accessible in one system; even considered separately, the E//c axis alone spans 124 nm and remains among the widest continuous tuning ranges reported for Yb-doped hosts. To the best of our knowledge, this positions Yb:YVO_4 among the most versatile gain media, surpassed only marginally by Yb:LuO (148 nm) [21]. These findings highlight Yb:YVO_4 as a promising gain medium for broad wavelength tuning, ultrashort pulse generation, and efficient seeding of cryogenic Yb:YLF amplifiers.

Optics EXPRESS

We note here that, in Fig. 1, we have only included the tuning of Yb-systems within their conventional fluorescence range. While Yb-doped gain media are generally limited to lasing within their fluorescence spectrum due to the dominance of direct electronic transitions, recent studies on Yb-doped YCOB [78] and LCB [28] gain media have shown that lasing far beyond this conventional range is possible via multiphonon-assisted transitions. However, such behavior relies on rare high-order phonon processes enabled by unique lattice structures and is not representative of typical Yb-doped materials, and is not included in Fig. 1.

The paper is structured as follows: Section 2 details the experimental setup; Sections 3 and 4 present the CW lasing and wavelength tuning results, respectively. Section 5 summarizes our findings, and the Appendix A provides additional analyses, including cavity-loss estimations, wavelength shifts associated with varying output coupler transmissions, temperature-dependent laser performance, and emission cross-section measurements.

2. Experimental setup

Figure 2 shows a schematic of the CW Yb:YVO_4 laser system used in the experiments with a detailed representation of the optical components for all tested configurations. A single-emitter multi-mode diode (MMD, LDX-3A10-960-C from RPMC Lasers), capable of delivering a maximum of 10 W of power, was used as the pump source. A pump wavelength slightly below the main absorption peak (~952 nm vs ~985 nm [8]) was selected to optimize short-wavelength lasing near 1 µm. The MMD has an emitter size of 1×100 µm (sagittal/fast × tangential/slow axes) and provides an asymmetric rectangular-shaped multi-transverse mode beam. To mode-match the MMD pump with the cavity mode, we begin by collimating it using a 4.5 mm focal length aspheric lens (f_1). A cylindrical lens with a focal length of 50 mm (f_z, acting on the fast axis) is placed after the collimator to reduce diode beam astigmatism. Then, an achromatic doublet with a focal length of 75 mm (f_2) focuses the pump beam, achieving a beam waist of approximately 30 µm × 90 µm inside the crystal.

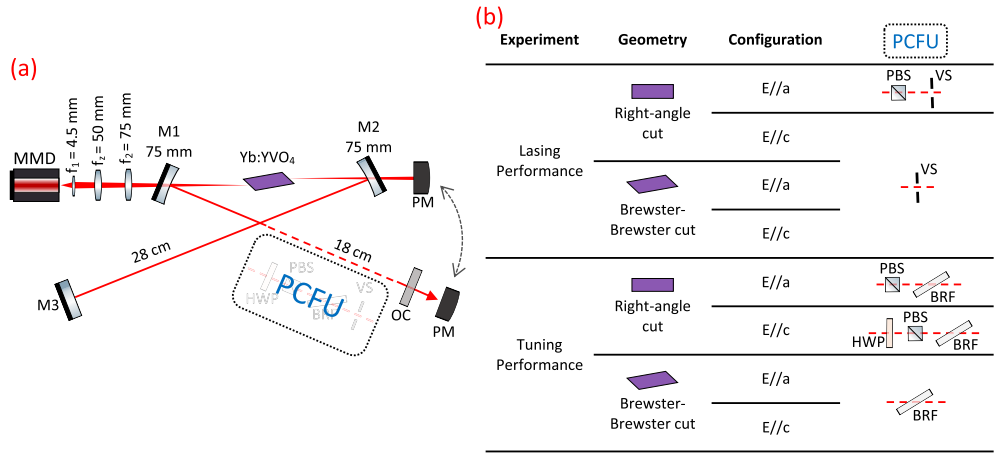

Fig. 2. (a) Experimental setup of the diode-pumped CW Yb:YVO_4 laser used in experiments. (b) Detailed representation of the optical components in the polarization control and filtering unit (PCFU) for the tested configurations. MMD: 10 W, 952 nm, single-emitter multimode laser pump diode; M: mirror; f: focusing lens; HWP: half-wave plate; PBS: polarizing beam splitter cube; BRF: birefringent filter; VS: variable slit; OC: output coupler; PM: power meter.

For the CW lasing experiments, three types of Yb:YVO_4 laser crystals were investigated: (i) a right-angle a-cut crystal to investigate lasing in both E//c and E//a configurations, (ii) a

Optics EXPRESS

Brewster-Brewster a-cut crystal for lasing in E//c configuration, and (iii) a Brewster-Brewster c-cut crystal for lasing in E//a configuration (Fig. 3(a-c)). Crystals are all 2.6% Yb-doped, 5 mm in length, 2 mm in width, and 2 mm in thickness. The right-angle a-cut crystal has anti-reflection coatings on both surfaces to minimize reflection for the pump and lasing wavelengths. When the crystal is positioned at a normal angle of incidence (as shown in Fig. 3(a)), the laser output can be selectively polarized as either TM (p) or TE (s). Without any additional intracavity elements, the laser emits in the E//c (s-polarization) configuration due to the higher gain in E//c (Fig. 7(d)). However, to force the laser to operate in the E//a (p-polarization) configuration, a PBS cube (which transmits p-polarized light and reflects s-polarized light) is integrated into the cavity (Fig. 2(b)). The Brewster-Brewster cut samples have no coatings, resulting in losses for TE (s) polarized light, which leads to laser output being primarily TM (p) polarized. Hence, the Brewster-Brewster cut samples shown in Fig. 3(a) and (b) lase in E//c and E//a axes, respectively. The crystals are mounted with indium foil in a water-cooled copper heat spreader. The water-cooling temperature is set to 10 °C. The estimated small-signal absorption for a 5 mm long Yb:YVO_4 crystal at 952 nm is 90% for the E//a axis and 73% for the E//c axis, due to the variation in absorption cross-section at the pump wavelength [8–10]. Consequently, the absorption of the Brewster-Brewster a-cut crystal used for E//c configuration is expected to be relatively low for TM-polarized pump light. Note that, due to the pump saturation [79], the effective absorption is further reduced below small-signal values in lasing conditions (measured at the maximum pump power level): 76% for the right-angle a-cut in E//c, 73% in right-angle a-cut in E//a, 56% in Brewster-Brewster a-cut in E//c, and 79% in Brewster-Brewster c-cut in E//a configurations, respectively.

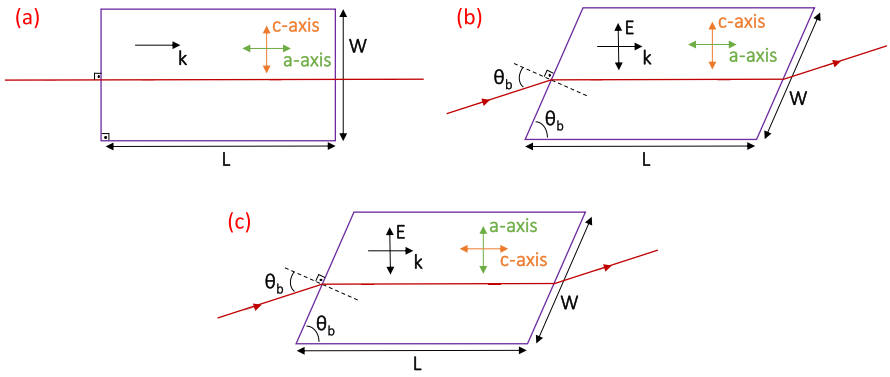

Fig. 3. Top view of the Yb:YVO_4 crystals used in experiments: (a) right-angle a-cut crystal (used selectively for both E//c and E//a configurations), and Brewster-Brewster cut crystals optimized for (b) E//c and (c) E//a lasing. The intracavity laser beam path is indicated in red. E: electric field vector for the intracavity laser beam; k: intracavity laser beam propagation direction; θ_b: Brewster's angle; L: length of the laser crystal; W: width of the crystal in the picture.

An X-type resonator configuration is employed, consisting of two curved high reflector mirrors with a radius of curvature of 75 mm (M1, M2), a flat high reflector (M3), and a flat output coupler (OC). The high reflector and output coupler arm lengths are set to be 28 cm and 18 cm, respectively. This configuration results in a beam waist of around 40 µm × 40 µm, 30 µm × 60 µm at the center of the right-angle and Brewster-Brewster cut crystals, respectively. Both dichroic mirrors, M1 and M2, have anti-reflection coatings optimized for the 800-970 nm range, ensuring that less than 2% of the incident light is reflected. All three high reflectors in the laser cavity, including M1, M2, and M3, have reflective coatings designed to cover the spectral range of 1010-1200 nm. These coatings are highly efficient, with a reflectivity exceeding 99.9% for 0°

Optics EXPRESS

incident light. Outside this range, the reflectivity does not drop rapidly; according to the company specifications (Layertec, 102924), the reflectivity remains above 99% down to 993 nm. To build an X-folded resonator, mirrors M1 and M2 are used at an incidence angle of around 10°, which slightly blue shifts the reflectivity band specified above. Fourteen different output couplers (OCs) with transmission ranging from 0.015% to 40% are used in the experiments to scan the lasing conditions range of the lasers. An adjustable-width mechanical slit is inserted near the output coupler to control the transverse output mode of the laser along the tangential axis to the optical table. For output wavelength tuning, a 2 mm-thick off-surface optical axis crystal quartz birefringent filter (BRF) with a diving angle of 25° was used. For the second order of the BRF, near a rotation angle of 35° and at an operating wavelength of around 1 μm, the filter exhibits a calculated free spectral range of approximately 350 nm, a full width at half-maximum (FWHM) transmission bandwidth of about 40 nm, and a tuning rate of roughly 45 nm per degree [80] The BRF is inserted at Brewster's angle; however, it was not enough to prevent polarization switches between p-polarization and s-polarization throughout the tuning range for the right-angle cut configurations. That's why, a PBS cube is implemented to ensure the laser consistently operates along the same axis. In contrast, for the Brewster-Brewster cut samples, there is no need for a PBS cube since the crystal geometry naturally introduces additional loss for s-polarized light. Note that, for the tuning in E//c configuration of the right-angle cut sample, an HWP was used before the PBS cube to rotate the polarization, to sustain lasing polarization (Fig. 2(b)).

The system diagnostics were performed using commercial measurement devices, including power meters (PM, Thorlabs S142C, Ophir Optronics FL250A-BB-35), spectrometers (Ocean Optics HR4000, and HR4000CG-UV-NIR), an optical spectrum analyzer (Yokogawa AQ6315A), and a beam profiler camera (DAT-WinCamD-LCM).

3. Continuous-wave lasing

With the experimental arrangement established, we now present the detailed CW lasing performance results across various cavity configurations and polarization axes. Figure 4(a-b) shows the measured power scaling curves of the Yb:YVO_4 laser for different output couplers with transmissions ranging from 0.015% to 30% for the right-angle cut crystal for E//c and E//a configurations, respectively. In the E//c configuration, the optimum CW performance was obtained with a 2% transmitting output coupler. Using this optimal output coupling, we measured a lasing threshold of around 1 W, and obtained a CW output power of 3.75 W at around 1046 nm wavelength at an absorbed pump power of 7.9 W (76% absorption). The laser reaches an optical-to-optical efficiency of 48%, and a slope efficiency of 70% at the optimal output coupling and maximum pump power level. For the E//a configuration (p-polarization), we placed a PBS cube into the cavity to suppress lasing in E//c. The PBS cube increased the overall cavity losses (Section A. 2). Due to the higher losses, the best CW performance was obtained with a 10% transmitting output coupler (Fig. 4(b)). At this output coupling, we measured a lasing threshold of around 1.3 W, and the laser produced a CW output power of 2.41 W around 1018 nm wavelength at an absorbed pump power of 7.6 W (73% absorption). The laser reaches an optical-to-optical efficiency of 32%, and a slope efficiency of 50% for the best output coupling at the maximum pump power level.

Laser performance measurements for the E//c and E//a configurations were repeated for the Brewster-Brewster cut samples as well. Figure 5(a) shows the power scaling curves in the E//c configuration using the Brewster-Brewster cut sample. Similar to the right-angle cut crystal, the optimum CW performance was obtained with a 2% transmitting OC. At this output coupling, we measured a lasing threshold of around 1.2 W, and the laser produced a maximum CW output power of 2.1 W around 1046 nm wavelength at an absorbed pump power of 5.8 W (56% absorption). The laser reaches an optical-to-optical efficiency of 37%, and a slope efficiency of 64% for the best output coupling at the maximum pump power level. The reason for the lower

Optics EXPRESS

performance compared to the right-angle a-cut crystal is the lower pump absorption due to the lower absorption cross-section in the E//c axis compared to the E//a axis at 952 nm [8–10].

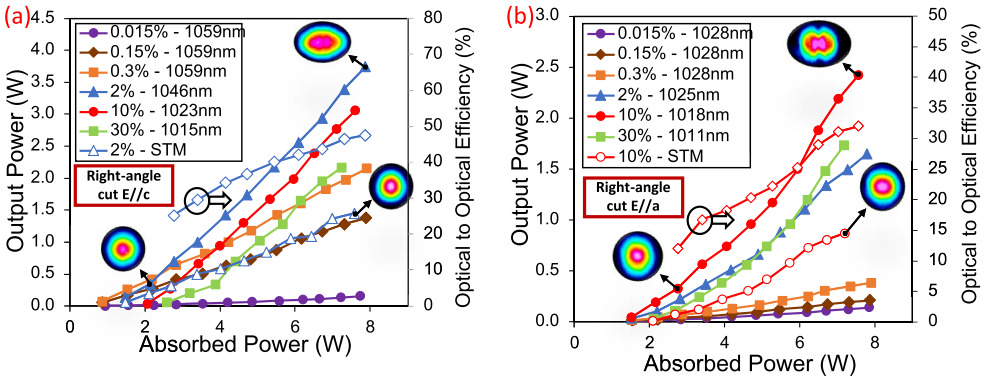

Fig. 4. CW laser performance of the room-temperature Yb:YVO_4 laser with OCs from 0.015% to 30%: (a) right-angle cut E//c and (b) E//a configurations. Insets show beam profiles at low and maximum power for optimal output coupling, both in free-running and forced single-transverse-mode (STM) operation. Optical-to-optical efficiency versus absorbed pump power is shown for the best-performing output couplers (2% OC for E//c, 10% OC for E//a).

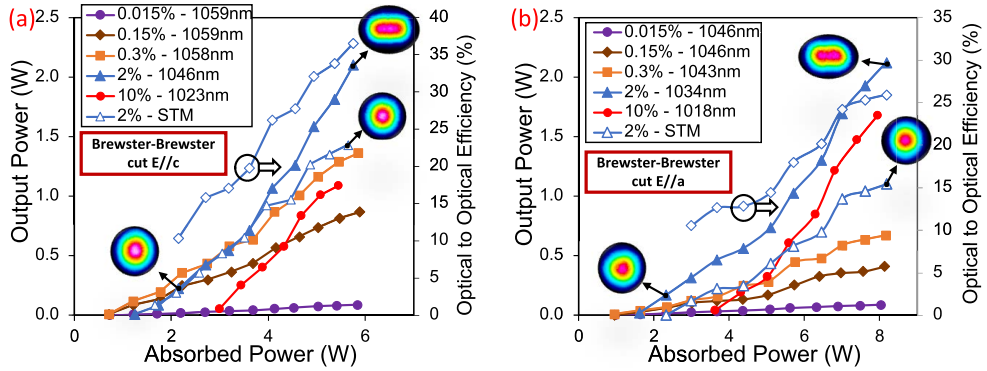

Fig. 5. Measured CW laser performance of the room-temperature Yb:YVO_4 laser using OCs in 0.015% to 10% range for Brewster-Brewster cut samples in (a) E//c and (b) E//a configurations.

Figure 5(b) shows the power scaling curves in the E//a configuration using the Brewster-Brewster cut sample. As the PBS was not required to suppress lasing in E//c axis, the cavity losses decreased, and the best CW performance was obtained with a 2% transmitting OC. At this output coupling, we measured a lasing threshold of around 1.6 W, and the laser produced a maximum CW output power of 2.1 W around 1034 nm wavelength at an absorbed pump power of 8.2 W (absorption, 79%). The laser reaches an optical-to-optical efficiency of 26%, and a slope efficiency of 36% for the best output coupling at the maximum pump power level. We realized that the reduced performance of the Brewster-Brewster cut sample compared to the right-angle cut crystal is due to an error in the cut angle of the Brewster-Brewster cut sample, resulting in depolarization losses (Section A. 2).

Optics EXPRESS

The insets in Figs. 4 and 5 display the near-field beam profiles of the CW Yb:YVO_4 laser at different pump power levels for the best-performing output couplers, which provide the highest slope efficiency. As the pump power increases, the laser output becomes multimode due to the multimode pump beam. However, single-transverse mode (STM) operation could be forced by adjusting the width of the variable slit placed near the OC mirror. In the forced STM operation, we have realized output power levels of 1.45 W, 0.87 W, 1.43 W, and 1.1 W for the right-angle cut E//c, right-angle cut E//a, Brewster-Brewster cut E//c, and Brewster-Brewster cut E//a configurations, respectively.

Further details on the CW lasing performance can be found in the Appendix: Section A. 1 is on the variation of free-running laser wavelength with output coupling, Section A. 2 is on the estimation of passive losses of the laser crystals and Section A. 3 is on the influence of cooling water temperature on the CW laser output power.

4. Continuous-wave laser wavelength tuning results

Having characterized the fundamental CW lasing parameters, we further explored the wavelength tuning potential, highlighting the broad spectral versatility of the Yb:YVO_4 gain medium. Figures 6 and 7 show the measured CW tuning performance of the room-temperature Yb:YVO_4 laser at an incident pump power of around 10 W for E//c and E//a configurations and both for the right-angle cut and Brewster-Brewster cut crystals. Tuning data were taken with several different output couplers with transmissions in the range of 0.015% to 20%. We have also

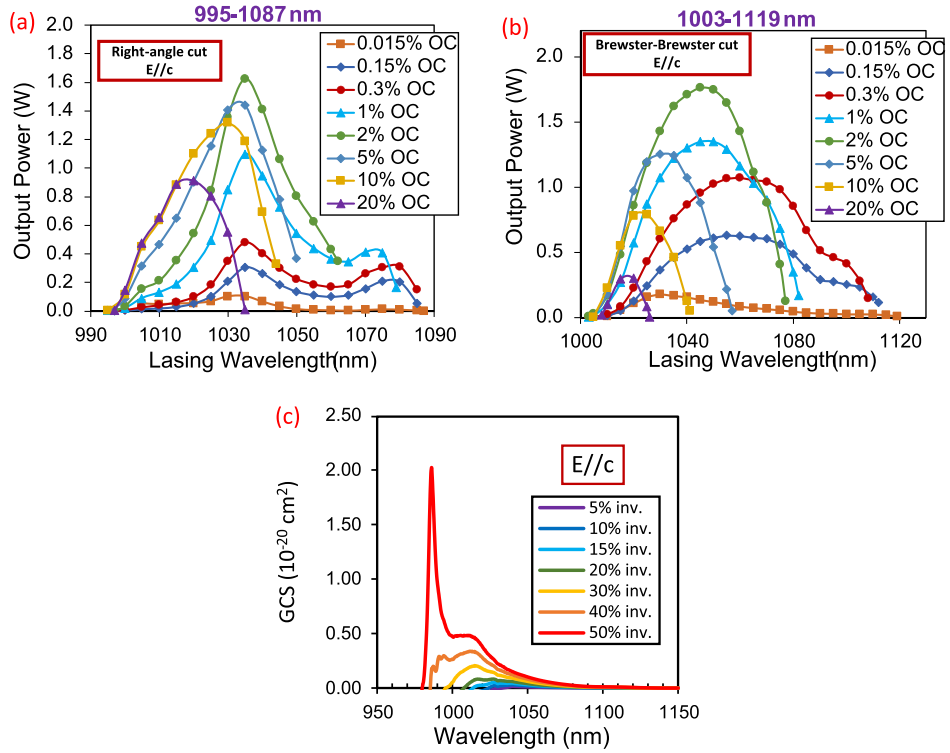

Fig. 6. Measured tuning behavior of the CW Yb:YVO_4 laser using output couplers in the 0.015% to 20% range for E//c configuration for the (a) right-angle cut, (b) Brewster-Brewster cut crystals. (c) Calculated room-temperature gain cross-section (GCS) spectra for Yb:YVO_4 at fractional population inversion levels (β) between 5 and 50% for the E//c axis.

Optics EXPRESS

included the calculated gain cross-section curves to the figures for a better understanding of the results. The room temperature gain cross-section (GCS, $\sigma_g(\lambda)$) was calculated, using the emission cross-section (ECS) obtained in this study, and the absorption cross-section (ACS) reported in [8] (see Appendix A. 4), by the following equation:

$$\sigma_g(\lambda) = \beta\sigma_e(\lambda) - (1-\beta)\sigma_a(\lambda), \tag{1}$$

where $\sigma_e(\sigma_a)$ is the emission (absorption) cross-section, and β is the fractional population inversion level. If we start from Fig. 6, which shows the obtained behavior for the E//c configuration, we see that for the right-angle cut and Brewster-cut crystals, the tuning behavior is different. In the case of the right-angle cut crystal, to enable lasing only in E//c configuration, a PBS cube and HWP pair were inserted into the cavity, which increases the overall losses. This, in turn, increases the required inversion to attain lasing. As we see from the calculated GCS curves in Fig. 6(c), this then results in favorable laser operation at shorter wavelengths. In comparison, for the Brewster-Brewster cut crystal, with lower cavity losses (as it does not require the PBS cube-HWP pair), one can operate the laser at lower inversion levels, especially when using low transmitting output couplers. Overall, we have demonstrated a CW tuning range covering the 995-1087 nm and 1003-1119 nm regions for the right-angle cut and Brewster-Brewster cut samples, respectively. The achieved power levels were above 1.5 W in the central region of the tuning. On the other hand, to achieve lasing on the edges of the gain curve, especially above

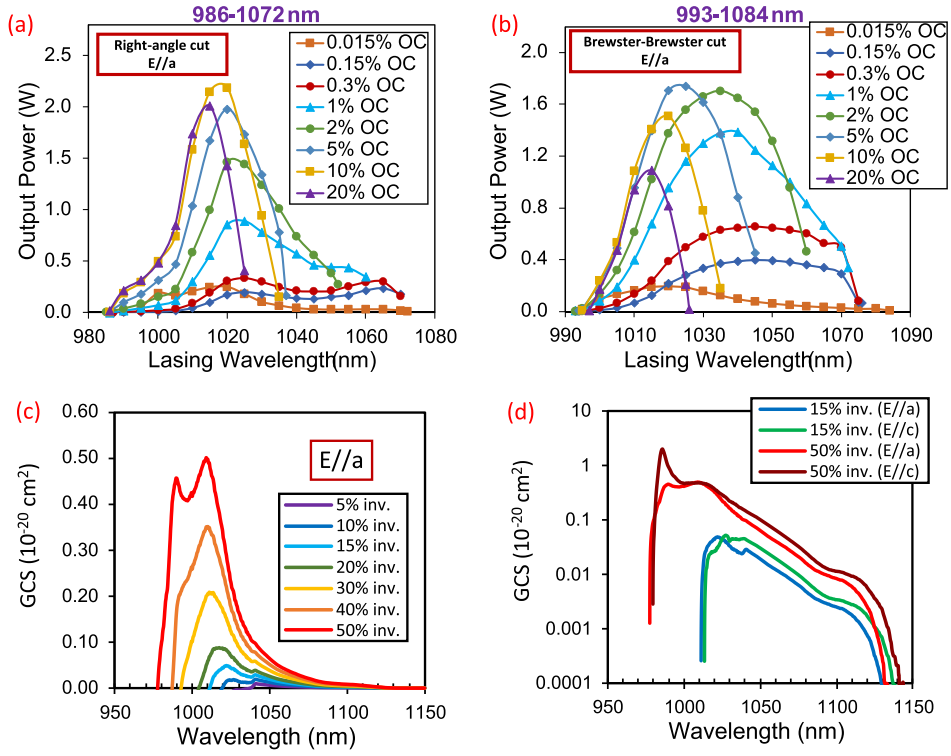

Fig. 7. CW tuning behavior of the Yb:YVO_4 laser (E//a polarization) for (a) right-angle and (b) Brewster-Brewster cut crystals, measured using output couplers with transmissions from 0.015% to 20%. (c) Calculated room-temperature gain cross-section (GCS) spectra for the E//a axis at fractional population inversion levels (β) of 5-50%. (d) Comparison of calculated GCS for E//c and E//a axes at β = 15% and 50%, shown on a logarithmic scale.

Optics EXPRESS

1100 nm, one needs to use output couplers with a lower transmission, which reduces the obtained output power levels to below 250 mW. Overall, as far as we are aware, the broadest reported earlier tuning for E//c axis of Yb:YVO_4 covers the 997-1074 nm spectral range [13]. With this result, we significantly extend the tuning range of Yb:YVO_4 toward longer wavelengths. We attribute this improvement to the use of low-loss optical components in our study; in particular, the internal passive loss of the laser crystal was estimated to be as low as 0.26% per centimeter (further details are provided in Section A. 2).

Figure 7 then shows the tuning behavior in E//a configuration, where we have demonstrated a tuning range of 986-1072 nm and 993-1084 nm for the right-angle cut and Brewster-Brewster cut samples, respectively. Similar to the E//c case, the difference between the right-angle cut and Brewster-Brewster cut samples can be attributed to the variation in the cavity losses, primarily due to the use of the PBS cube in the right-angle cut configuration. Overall, the trends observed are similar to the case of E//c discussed above. To our knowledge, there has been relatively limited investigation into wavelength tuning along the E//a axis of Yb:YVO_4. Previously reported tuning ranges have been confined to the 1021–1036 nm region [16]. Our results with E//a axis show that broad tuning could also be achieved in Yb:YVO_4 in E//a configuration. For comparison of E//c and E//a axes, Fig. 7(d) shows the GCS curve for both axes in the same graph at selected inversion levels of 15% and 50% in the logarithmic scale. For the long wavelength side, the E//c axis gain spectra extend to longer wavelengths compared to E//a configuration (for a fixed inversion level), and this explains the slightly extended longer wavelength tuning limit we have achieved while employing the E//c polarization (1087 nm in E//c versus 1072 nm in E//a using the right-angle a-cut crystal). We close this section, with Fig. 8 which shows sample optical spectra taken during the CW tuning experiments of the Yb:YVO_4 laser in the 986-1119 nm region.

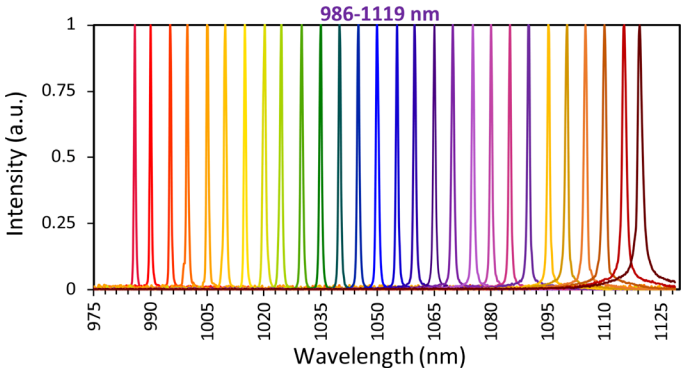

Fig. 8. Sample optical spectra demonstrating CW tunability of the Yb:YVO_4 laser for the overall tuning range covering the 986-1119 nm region.

5. Conclusion

We have studied the continuous-wave tuning performance of 2.6% Yb-doped YVO_4 crystals in various configurations at room temperature using a diode-pumped laser system. Our experiments yielded a broad CW tuning range from 986 to 1119 nm, representing one of the broadest CW tuning ranges obtained from any studied Yb-doped gain media to date. The system also demonstrated a maximum CW power of 3.75 W with a slope efficiency of 70% and optical-to-optical efficiency of 48%. These findings show the potential of Yb:YVO_4 host in ultrafast laser generation and amplification. Future efforts will be focused on using the Yb:YVO_4 system as a seed source to take advantage of the gain peak of cryogenic Yb:YLF at 995 nm [7].

Optics EXPRESS

Appendix A

For further insights into critical aspects of our laser system that significantly impact performance and operational characteristics, such as estimations of cavity passive losses, detailed analysis of wavelength shifts associated with varying output coupler transmissions, and the influence of crystal temperature on laser output power, additional comprehensive analyses and discussions are provided in the Appendix. Additionally, to accurately model and interpret the gain behavior across the full tuning range, we have measured the room-temperature emission cross-sections of Yb:YVO_4. These supplementary studies offer a deeper understanding of the system's internal dynamics and practical considerations for optimizing future laser designs.

A1. Variation of free-running laser wavelength with output coupler value

As mentioned in earlier sections, the optimal output coupling for low-loss Yb:YVO_4 laser cavities typically lies around 2%, whereas broader wavelength tuning demands lower output coupling values, around 0.5%. In this subsection, we provide additional detailed analysis to clarify these findings. Figure 9 illustrates the variation in free-running laser wavelength and maximum CW output power as functions of output coupling for all investigated configurations. Note that some data points presented here were not included in Figs. 4–7 to maintain the clarity and readability of those plots. A consistent trend emerges across all configurations: as the output coupling increases, the free-running laser wavelength shifts toward shorter wavelengths (blue-shift). This behavior arises from fundamental gain dynamics; increasing cavity losses necessitate higher population inversion levels to achieve the lasing threshold. Higher inversion levels, in turn, shift the gain peak to shorter wavelengths, as clearly seen in the gain cross-section curves (Figs. 6(c) and 7(c)) [8–10]. Additionally, we observe that while both E//c configurations exhibit comparable wavelength trends, the right-angle cut E//a configuration consistently lases at shorter wavelengths than the Brewster-Brewster cut E//a configuration for all output couplings. This discrepancy results from elevated passive losses introduced by the additional polarizing beam splitter (PBS) required in the right-angle cut E//a setup, highlighting the critical role of cavity losses in determining laser emission characteristics.

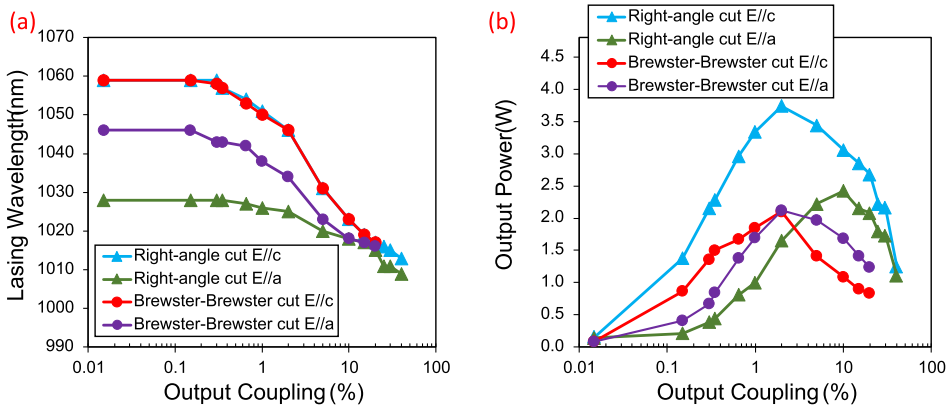

Fig. 9. Measured variation of (a) free-running lasing wavelength and (b) maximum CW output power for different output coupling transmissions for various configurations. The data were taken while pumping the room-temperature Yb:YVO_4 laser at an incident pump power of 10 W.

Furthermore, at all tested output coupling values, we observe that the free-running laser wavelengths consistently appear longer in the E//c configuration compared to the E//a configuration.

Optics EXPRESS

For instance, with a 0.015% transmitting output coupler, the Brewster-Brewster cut crystal lases at 1059 nm in the E//c configuration, while it shifts to 1046 nm in the E//a configuration. This phenomenon is primarily due to the inherently lower gain cross-section along the E//a axis, as depicted in Fig. 7(d). The reduced gain cross-section necessitates a higher inversion level for achieving the lasing threshold, resulting in a systematic shift of the emission to shorter wavelengths (blue shift) relative to the E//c configuration.

A2. Estimation of the passive losses of the crystals

We estimated the passive cavity losses from the measured laser slope efficiencies using Caird analysis [81]. Based on the best fits (Fig. 10), the estimated round-trip passive losses are 2.50%, 0.32%, 1.05%, and 0.42% for right-angle cut E//a, right-angle cut E//c, Brewster-Brewster cut E//a, and Brewster-Brewster cut E//c configurations, respectively. Although similar loss values would normally be expected for the right-angle cut configurations (since the same crystal is used), the E//a configuration required an additional polarizing beam splitter (PBS) to suppress competing lasing along the E//c axis. By comparing these two configurations, we determined that the PBS introduces approximately 1.09% loss per pass. Accounting for minor cavity optics losses (~0.06%), we estimate the intrinsic passive losses of the Yb:YVO_4 crystals as 0.26%/cm for the right-angle cut, 0.36%/cm for the Brewster-Brewster cut (E//c), and 0.99%/cm for the Brewster-Brewster cut (E//a). The significantly higher loss observed for the Brewster-Brewster E//a crystal likely originates from depolarization losses caused by slight misalignments in the crystal orientation or imperfect parallelism of the crystal faces. To minimize these losses, we recommend using a Brewster-Brewster a-cut crystal specifically optimized for E//a-axis lasing in future experiments. However, if achieving higher output powers is the primary goal, our findings suggest that using a right-angle cut crystal, pumped along E//a and lasing along E//c, is the most efficient configuration.

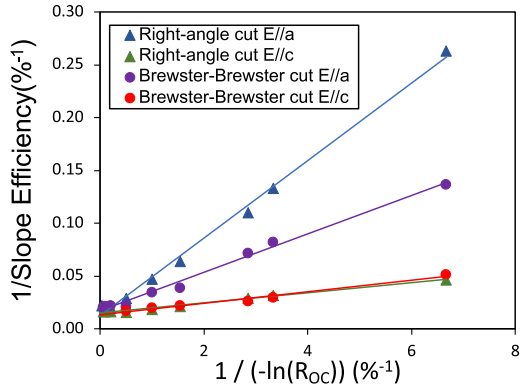

Fig. 10. Variation of the inverse of the slope efficiency with the inverse of the output coupling percentage for the right-angle a-cut E//a, right-angle a-cut E//c, Brewster-Brewster c-cut E//a, and Brewster-Brewster a-cut E//c configurations. For the slope efficiency values, a linear fit is made to the laser power scaling curves for the data points above the 4 W absorbed pump power level.

A3. Influence of cooling water temperature on the laser performance

Figure 11 illustrates the dependence of the CW output power of the Yb:YVO_4 laser on the cooling water temperature in the range of 10-50 °C, using the right-angle cut crystal in both principal polarization configurations (E//a and E//c). Measurements were performed at a constant

Optics EXPRESS

incident pump power of 10 W, employing optimal output couplers, 2% for E//c and 10% for E//a, respectively. As the temperature of the crystal holder increases, the maximum achievable output power gradually decreases in both configurations. This behavior primarily results from the temperature-dependent decrease in the gain cross-section. Linear fits to the measured data reveal output power reductions of approximately 3‰/°C for the E//c axis and 5‰/°C for the E//a axis. Despite this linear trend, the observed reductions are relatively modest, clearly indicating that the maximum output power of 3.75 W achieved in our experiments is predominantly limited by available pump power rather than thermal constraints. Consequently, future investigations employing higher-power diode sources under similar experimental conditions could readily achieve substantially higher output power levels.

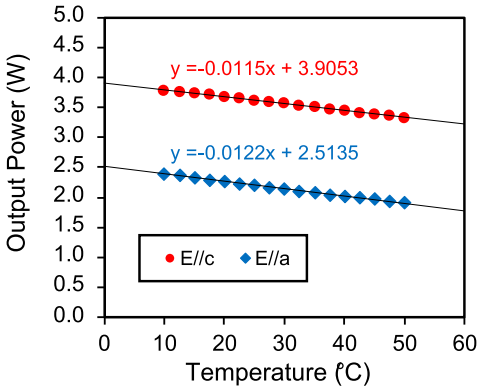

Fig. 11. Measured variation of Yb:YVO_4 laser output power with the cooling water temperature. The data were taken at an incident pump power of 10 W using 2% and 10% transmitting output couplers for the right-angle a cut E//c, and E//a configurations, respectively. The linear fits for the data points are also shown with the relevant equations.

A4. Room temperature emission cross-section of Yb:YVO_4

The literature lacks emission cross-section data for Yb:YVO_4 beyond 1080 nm [8–10]. In order to calculate the gain cross-section for the full wavelength tuning range, we have measured the polarization-dependent photoluminescence spectrum and derived the ECS using the well-established Füchtbauer-Ladenburg approach, accounting for possible self-absorption losses like in [82]. Figure 12 presents the resulting emission cross-sections for both E//a and E//c polarization configurations, extending up to 1150 nm, and compares them with existing literature values. The results show good agreement within the overlapping regions, while providing, according to existing studies, the first ECS data for Yb:YVO_4 in the long-wavelength range. For completeness, the literature absorption cross-section (ACS, [8]) values used in the gain calculations are also included in the figure.

Optics EXPRESS

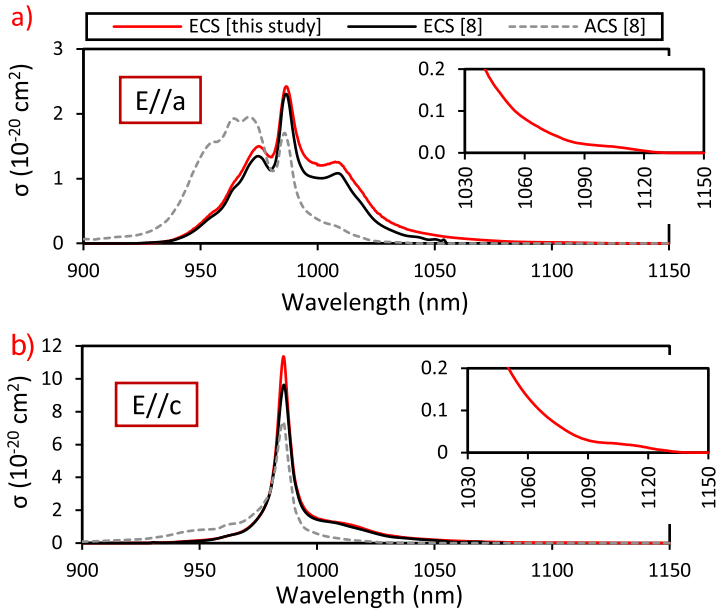

Fig. 12. Emission cross-section of room-temperature Yb:YVO_4 obtained in this study, compared with literature values, and the absorption cross-sections used for gain calculations, for (a) E//a and (b) E//c configurations.

Funding. European Research Council (609920); Deutsches Elektronen-Synchrotron DESY; Helmholtz Association of German Research Centres Program MML-Matter.

Disclosures. The authors declare no conflicts of interest.

Data availability. Data underlying the results presented in this paper are not publicly available at this time but may be obtained from the authors upon reasonable request.

References

1. F. J. Duarte, *Tunable Laser Applications* (CRC Press, 2016).
2. T. Farrell and D. McDonald, "Tunable laser technology for sensing applications," in *Physics and Applications of Optoelectronic Devices* (SPIE, 2004), 5594, p. 66.
3. L. G. Shirley, G. R. Hallerman, and L. Laboratory, *Applications of Tunable Lasers to Laser Radar and 3D Imaging* (1996).
4. B. Pezeshki, G. Parhar, and N. Badr, "Tunable Lasers," IEEE Circuits Devices Mag. **19**(5), 36–40 (2003).
5. S.-L. Lee, Y.-T. Pan, Y.-J. Hung, *et al.*, "Trend and applications of tunable semiconductor lasers," in *Optoelectronic Materials and Devices II* (SPIE, 2007), 6782, p. 67821H.
6. R. F. Curl and F. K. Tittel, "Tunable infrared laser spectroscopy," Annu. Rep. Prog. Chem., Sect. C: Phys. Chem. **98**, 219–272 (2002).
7. U. Demirbas, J. Thesinga, M. Kellert, *et al.*, "Detailed investigation of absorption, emission and gain in Yb:YLF in the 78–300 K range," Opt. Mater. Express **11**(2), 250 (2021).
8. V. E. Kisel, A. E. Troshin, N. A. Tolstik, *et al.*, "Spectroscopy and continuous-wave diode-pumped laser action of Yb^{3+}:YVO_4," Opt. Lett. **29**(21), 2491 (2004).
9. C. Kränkel, D. Fagundes-Peters, S. T. Fredrich, *et al.*, "Continuous wave laser operation of Yb^{3+}:YVO_4," Appl. Phys. B **79**(5), 543–546 (2004).
10. D. Zhong, B. Teng, J. Li, *et al.*, "Growth and laser action of Yb: YVO_4 crystals with low Yb doping concentration," J. Cryst. Growth **358**(1), 16–19 (2012).
11. M. Pergament, M. Kellert, U. Demirbas, *et al.*, "100-mJ, 100-W cryogenically cooled Yb:YLF laser," Opt. Lett. **48**(11), 2833 (2023).
12. M. Kilinc, U. Demirbas, J. Thesinga, *et al.*, "Pushing the tuning limits of femtosecond Yb-based solid-state lasers to 1 µm: a Yb:YVO_4 laser tunable down to 1004 nm," Opt. Lett. **49**(18), 5236–5239 (2024).
13. A. Rudenkov, V. Kisel, V. Matrosov, *et al.*, "200 kHz 55 W Yb^{3+}: YVO_4-based chirped-pulse regenerative amplifier," Opt. Lett. **40**(14), 3352 (2015).

Optics EXPRESS

14. C. Kränkel, R. Peters, K. Petermann, *et al.*, "High Power Operation of Yb:$LuVO_4$ and Yb:YVO_4 Crystals in the Thin-Disk Laser Setup," in *Advanced Solid-State Photonics* (OSA, 2007), p. MA3.
15. X. Tian, Zh. Zhou, Q. Dai, *et al.*, "Study of Yb:YVO_4 lasers end-pumped by a 985-nm diode laser," Laser Phys. **22**(4), 688–692 (2012).
16. J. Liu, W. Han, H. Zhang, *et al.*, "Comparative study of high-power continuous-wave laser performance of Yb-doped vanadate crystals," IEEE J. Quantum Electron. **45**(7), 807–815 (2009).
17. V. E. Kisel, A. E. Troshin, N. A. Tolstik, *et al.*, "Continuous-wave, Q-switched and mode-locked laser operation of Yb^{3+} -doped YVO_4 single crystal," in *Advanced Solid-State Photonics (TOPS)* (OSA, 2005), p. 145.
18. F. M. Bain, A. A. Lagatsky, C. T. A. Brown, *et al.*, "High-power Kerr-lens mode-locked ytterbium lasers," in *Solid State Lasers XVII: Technology and Devices* (SPIE, 2008), 6871, p. 68712L.
19. X. H. Li, X. W. Chen, W. J. Han, *et al.*, "Passive Q-switching laser performance of Yb:YVO_4 crystal," Chin. Phys. Lett. **31**(12), 124202 (2014).
20. K. Naganuma, G. Lenz, and E. P. Ippen, "Variable bandwidth birefringent filter for stable femtosecond lasers," IEEE J. Quantum Electron. **28**(10), 2142–2150 (1992).
21. R. Peters, C. Kränkel, K. Petermann, *et al.*, "Broadly tunable high-power Yb:Lu_2O_3 thin disk laser with 80% slope efficiency," Opt. Express **15**(11), 7075 (2007).
22. A. Rudenkov, V. Kisel, A. Yasukevich, *et al.*, "Spectroscopy and continuous wave laser performance of Yb^{3+}:$LuAlO_2$ crystal," Opt. Lett. **41**(24), 5805 (2016).
23. M. Jacquemet, C. Jacquemet, N. Janel, *et al.*, "Efficient laser action of Yb:LSO and Yb:YSO oxyorthosilicates crystals under high-power diode-pumping," Appl. Phys. B **80**(2), 171–176 (2005).
24. G. Toci, A. Pirri, A. Beitlerova, *et al.*, "Characterization of the lasing properties of a 5% Yb doped Lu_2SiO_5 crystal along its three principal dielectric axes," Opt. Express **23**(10), 13210 (2015).
25. C. Kränkel, J. Johannsen, R. Peters, *et al.*, "Continuous-wave high power laser operation and tunability of Yb:$LaSc_3(BO_3)_4$ in thin disk configuration," Appl. Phys. B **87**(2), 217–220 (2007).
26. K. S. Wentsch, B. Weichelt, S. Günster, *et al.*, "Yb:CaF_2 thin-disk laser," Opt. Express **22**(2), 1524 (2014).
27. U. Demirbas, J. Thesinga, M. Kellert, *et al.*, "Broadly tunable (993–1110 nm) Yb:YLF laser," Appl. Opt. **61**(13), 3702 (2022).
28. Y. Cheng, F. Liang, D. Lu, *et al.*, "Phonon engineering in Yb:$La_2CaB_{10}O_{19}$ crystal for extended lasing beyond the fluorescence spectrum," Light: Sci. Appl. **12**(1), 203 (2023).
29. B. Jacobsson, J. E. Hellström, V. Pasiskevicius, *et al.*, "Widely tunable Yb:KYW laser with a volume Bragg grating," Opt. Express **15**(3), 1003 (2007).
30. H.-J. Zeng, Z.-L. Lin, G. Zhang, *et al.*, "Diode-pumped mode-locked Yb:$Ca_3La_2(BO_3)_4$ laser generating 35 fs pulses," Opt. Express **33**(11), 22988 (2025).
31. K. Beil, B. Deppe, and C. Kränkel, "Yb:$CaGdAlO_4$ thin-disk laser with 70% slope efficiency and 90 nm wavelength tuning range," Opt. Lett. **38**(11), 1966 (2013).
32. X. Liu, X. Li, H. Nie, *et al.*, "Growth, micromechanical aspects, spectroscopy, and laser performance of Yb: CALGO crystal," Opt. Laser. Technol. **189**, 113140 (2025).
33. M. Jacquemet, F. Balembois, S. Chneais, *et al.*, "First diode-pumped Yb-doped solid-state laser continuously tunable between 1000 and 1010 nm," Appl. Phys. B **78**(1), 13–18 (2004).
34. W. Li, Q. Hao, H. Zhai, *et al.*, "Low-threshold and continuously tunable Yb:Gd_2SiO_5 laser," Appl. Phys. Lett. **89**(10), 101125 (2006).
35. H.-J. Zeng, Z.-L. Lin, Z. Pan, *et al.*, "Continuous-wave and passively mode-locked operation of Yb:$Ca_3Gd_2(BO_3)_4$ laser," in *Solid State Lasers XXXI: Technology and Devices*, W. A. Clarkson and R. K. Shori, eds. (SPIE, 2022), p. 44.
36. H. Z. Hanyin Zhang, J. L. Jinfeng Li, X. L. Xiaoyan Liang, *et al.*, "High-power and wavelength tunable diode-pumped continuous wave Yb:SSO laser," Chin. Opt. Lett. **10**(11), 111404 (2012).
37. L. Dong, Z.-L. Lin, P. Loiko, *et al.*, "Diode-pumped mode-locked Yb:Sc_2SiO_5 laser generating 38 fs pulses," Opt. Express **31**(8), 12463 (2023).
38. H. Zeng, H. Lin, Z. Lin, *et al.*, "Diode-pumped sub-50-fs Kerr-lens mode-locked Yb:GdYCOB laser," Opt. Express **29**(9), 13496 (2021).
39. A. Garcia-Cortes, J. M. Cano-Torres, M. D. Serrano, *et al.*, "Spectroscopy and lasing of Yb-doped $NaY(WO_4)_2$: tunable and femtosecond mode-locked laser operation," IEEE J. Quantum Electron. **43**(9), 758–764 (2007).
40. X. Yin, G. Wu, S. Fan, *et al.*, "All-solid-state widely wavelength-tunable and high-efficiency Yb:$YSr_3(PO_4)_3$ laser," Appl. Opt. **60**(22), 6713 (2021).
41. Z.-Q. Li, Z.-L. Lin, H.-J. Zeng, *et al.*, "Continuous-wave and SESAM mode-locked operation of a Yb:$YSr_3(PO_4)_3$ laser," Opt. Express **32**(3), 3974 (2024).
42. J. Zhu, Z. Gao, W. Tian, *et al.*, "Kerr-lens mode-locked femtosecond Yb:$GdYSiO_5$ laser directly pumped by a laser diode," Applied Sciences **5**(4), 817–824 (2015).
43. A. Schmidt, S. Rivier, V. Petrov, *et al.*, "Continuous-wave tunable and femtosecond mode-locked laser operation of Yb:$NaY(MoO_4)_2$," J. Opt. Soc. Am. B **25**(8), 1341 (2008).
44. J. Šulc, O. Krivosudský, H. Jelínková, *et al.*, "Tunability of Yb:glass laser," in *Solid State Lasers XXII: Technology and Devices*, W. A. Clarkson and R. Shori, eds. (SPIE, 2013), 8599, p. 85991U.
45. T. Danger, E. Mix, E. Heumann, *et al.*, "Diode pumped continuous-wave Yb laser in fluoride phosphate glasses," in *Advanced Solid State Lasers* (OSA, 1996), p. YL6.

Optics EXPRESS

46. M. Loeser, F. Röser, A. Reichelt, *et al.*, "Broadband, diode pumped Yb:SiO_2 multicomponent glass laser," Opt. Lett. **37**(19), 4029 (2012).
47. W.-Z. Xue, P. Loiko, Z.-L. Lin, *et al.*, "Sub-50 fs diode-pumped SESAM mode-locked Yb:SrF_2 laser," Opt. Express **31**(10), 16634 (2023).
48. M. Rumpel, A. Voss, M. Moeller, *et al.*, "Linearly polarized, narrow-linewidth, and tunable Yb:YAG thin-disk laser," Opt. Lett. **37**(20), 4188 (2012).
49. A. Baum, D. Grebner, W. Paa, *et al.*, "Axial mode tuning of a single frequency Yb:YAG thin disk laser," Appl. Phys. B **81**(8), 1091–1096 (2005).
50. W.-Z. Xue, Z.-L. Lin, H.-J. Zeng, *et al.*, "Diode-pumped mode-locked Yb:BaF_2 laser," Opt. Express **30**(9), 15807 (2022).
51. A. Yoshida, A. Schmidt, H. Zhang, *et al.*, "42-fs diode-pumped Yb:$Ca_4YO(BO_3)_3$ oscillator," Opt. Express **18**(23), 24325 (2010).
52. Y. Xue, C. Wang, J. Li, *et al.*, "A highly efficient and widely tunable bifunctional Yb:GdYAB laser," IEEE J. Quantum Electron. **44**(7), 686–691 (2008).
53. A. García-Cortés, J. M. Cano-Torres, X. Han, *et al.*, "Tunable continuous wave and femtosecond mode-locked Yb^{3+} laser operation in $NaLu(WO_4)_2$," J. Appl. Phys. **101**(6), 063110 (2007).
54. H. Lin, Z. Lin, Y. Chen, *et al.*, "Continuous-wave and SESAM mode-locked operation of the Yb:Bi_4Si_{312} laser," Opt. Express **29**(1), 105 (2021).
55. P. Zhang, W. Wu, Z.-L. Lin, *et al.*, "Growth, spectroscopy and SESAM mode-locking of a "mixed" Yb:Ca(Gd,Y)AlO_4 disordered crystal," Opt. Express **32**(3), 3221 (2024).
56. W.-Z. Xue, Z.-L. Lin, H.-J. Zeng, *et al.*, "Diode-pumped SESAM mode-locked Yb:(Y,Gd)AlO_3 laser," Opt. Express **30**(7), 11825 (2022).
57. H.-J. Zeng, Z.-L. Lin, W.-Z. Xue, *et al.*, "SESAM mode-locked Yb:$SrLaAlO_4$ laser," Opt. Express **29**(26), 43820 (2021).
58. Z.-L. Lin, P. Loiko, H.-J. Zeng, *et al.*, "Kerr-lens mode-locking of an Yb:CLNGG laser," Opt. Express **31**(5), 8575 (2023).
59. F. Augé, F. Balembois, P. Georges, *et al.*, "Efficient and tunable continuous-wave diode-pumped Yb^{3+}:$Ca_4GdO(BO_4)_3$ laser," Appl. Opt. **38**(6), 976 (1999).
60. C. Cascales, M. D. Serrano, F. Esteban-Betegón, *et al.*, "Structural, spectroscopic, and tunable laser properties of Yb^{3+}-doped $NaGd(WO_4)_2$," Phys. Rev. B **74**(17), 174114 (2006).
61. Z. Zhang, Z.-Q. Li, P. Loiko, *et al.*, "35-fs diode-pumped mode-locked ytterbium-doped multi-component alkaline-earth fluoride laser," Opt. Lett. **50**(6), 1835 (2025).
62. W. Li, S. Xu, H. Pan, *et al.*, "Efficient tunable diode-pumped Yb:LYSO laser," Opt. Express **14**(15), 6681 (2006).
63. J. Du, X. Liang, Y. Xu, *et al.*, "Continuous-wave diode-pumped Yb^{3+}:LYSO tunable laser," in *27th International Congress on High-Speed Photography and Photonics*, X. Hou, W. Zhao, and B. Yao, eds. (SPIE, 2007), 6279, p. 627963.
64. M. Rico, U. Griebner, V. Petrov, *et al.*, "Growth, spectroscopy, and tunable laser operation of the disordered crystal $LiGd(MoO_4)_2$ doped with ytterbium," J. Opt. Soc. Am. B **23**(6), 1083 (2006).
65. M. Rico, J. Liu, J. M. Cano-Torres, *et al.*, "Continuous wave and tunable laser operation of Yb^{3+} in disordered $NaLa(MoO_4)_2$," Appl. Phys. B **81**(5), 621–625 (2005).
66. S. Sun, H.-J. Zeng, Z.-L. Lin, *et al.*, "SESAM mode-locked Yb:$Sr_3Y_2(BO_3)_4$ laser," Opt. Express **30**(7), 11861 (2022).
67. P. Dekker, P. A. Burns, J. M. Dawes, *et al.*, "Widely tunable yellow-green lasers based on the self-frequency-doubling material Yb:YAB," J. Opt. Soc. Am. B **20**(4), 706 (2003).
68. S. Chénais, F. Druon, F. Balembois, *et al.*, "Spectroscopy and efficient laser action from diode pumping of a new broadly tunable crystal: Yb^{3+}:Sr_3 $Y(BO_3)_3$," J. Opt. Soc. Am. B **19**(5), 1083 (2002).
69. M. Stehlík, J. Šulc, P. Boháček, *et al.*, "Wavelength tunability of laser based on Yb-doped GGAG crystal," Laser Phys. **28**(10), 105802 (2018).
70. H.-J. Zeng, Z.-L. Lin, P. Loiko, *et al.*, "Spectroscopy and SESAM mode-locking of a disordered Yb:Gd $_2$ SrAl $_2$ O $_7$ crystal," Opt. Express **33**(7), 15057 (2025).
71. Y. Zhu, M. Xiong, Y. Han, *et al.*, "The first demonstration of wavelength-tunable Yb^{3+}-doped low silica calcium aluminosilicate (LSCAS) glass lasers," Infrared Phys. Technol. **137**, 105144 (2024).
72. H.-Y. Nie, Z.-L. Lin, P. Loiko, *et al.*, "Diode-pumped Kerr-lens mode-locked Yb:$MgWO_4$ laser," Opt. Lett. **50**(3), 1049 (2025).
73. A. Brenier, Y. Guyot, H. Canibano, *et al.*, "Growth, spectroscopic, and laser properties of Yb^{3+}-doped $Lu_3Al_5O_{12}$ garnet crystal," J. Opt. Soc. Am. B **23**(4), 676 (2006).
74. J. Suie, J. Mesicek, Z. Hubka, *et al.*, "Tunability of Yb:LuAG laser with high dopant concentration," in *2013 Conference on Lasers & Electro-Optics Europe & International Quantum Electronics Conference CLEO EUROPE/IQEC* (IEEE, 2013), 17, pp. 1.
75. S. Slimi, P. Loiko, M. Pan, *et al.*, "Growth, structure, spectroscopy, and laser operation of a "mixed" Yb:$(Y,Lu)_3Al_5O_{12}$ garnet crystal," Crystals **13**(11), 1588 (2023).
76. J. Guo, S. Li, C. Zhao, *et al.*, "SESAM mode-locked Yb:$GdScO_3$ laser," Opt. Express **32**(5), 7865 (2024).

Optics EXPRESS

77. E. Montoya, J. A. Sanz-García, J. Capmany, *et al.*, "Continuous wave infrared laser action, self-frequency doubling, and tunability of Yb^{3+}:MgO:$LiNbO_3$," J. Appl. Phys. **87**(9), 4056–4062 (2000).
78. F. Liang, C. He, D. Lu, *et al.*, "Multiphonon-assisted lasing beyond the fluorescence spectrum," Nat. Phys. **18**(11), 1312–1316 (2022).
79. L. Cheng, L. B. Andre, G. L. Almeida, *et al.*, "Differential absorption saturation in laser cooled Yb:$LiYF_4$," Opt. Mater. **128**, 112404 (2022).
80. U. Demirbas, "Off-surface optic axis birefringent filters for smooth tuning of broadband lasers," Appl. Opt. **56**(28), 7815 (2017).
81. J. A. Caird, S. A. Payne, P. R. Staber, *et al.*, "Quantum electronic properties of the $Na_3Ga_2Li_3F_{12}$:Cr^{3+} laser," IEEE J. Quantum Electron. **24**(6), 1077–1099 (1988).
82. T. Y. Fan, D. J. Ripin, R. L. Aggarwal, *et al.*, "Cryogenic Yb^{3+}-doped solid-state lasers," IEEE J. Select. Topics Quantum Electron. **13**(3), 448–459 (2007).